The Role of Hydrogen Bonding in the Crystal Structures of Zinc Phosphate Hydrates

Laurent Herschke, Volker Enkelmann, Ingo Lieberwirth,* and Gerhard Wegner[a]

Abstract: The compounds α- and β-hopeite have been synthesised by hydrothermal crystallisation from aqueous solution at 90 °C and 20 °C, respectively. The crystal structures of these polymorphic forms of zinc phosphate tetrahydrate (ZPT), $Zn_3(PO_4)_2{\cdot}4H_2O$, have been resolved. Single-crystal analysis proves that the main difference between the α and β forms of ZPT is caused by the difference in orientation of one of the water molecules in the ZnO_6 octahedral network, indicating two different hydrogen-bonding patterns. A previously unknown hopeite, $Zn_3(HPO_4)_3{\cdot}3H_2O$ (ZHPT), has been isolated and analysed. This helps to achieve a better understanding of the mechanism of formation of zinc phosphate compounds. Unambiguous identification of each phase is established by analysis of their unique thermal behaviour and thermodynamic interrelationship.

Keywords: hopeite · hydrogen bonds · polymorphism · structure elucidation · zinc phosphate

Introduction

Painting is an effective way to protect metallic surfaces against aggressive environments. Red lead and zinc chromate are the most extensively used pigments, because of their excellent corrosion inhibition properties. Nevertheless, since 1990 their use has been discouraged because it is hazardous and such compounds are highly toxic.[1] Manufacturing effort is focused on their replacement with a new generation of "environmentally friendly" pigments.[2–5]

Among several nontoxic anticorrosive pigments developed so far, zinc phosphate types represent the most widely employed alternative, although their anticorrosive action is not yet understood. It seems that the protective mechanism results from metal substrate phosphatisation[6,7] and formation of complex substances with the binder components.[8] Such compounds react with oxidation products yielding an adherent layer of phosphophyllite on the metal surface.[9,10] Accordingly their anticorrosive efficiency depends on water uptake.[11] Among the major limitations of zinc phosphate pigments as corrosion inhibitors are their poor solubility[12,13] and the difficulty of controlling the desired state of hydration.[14]

In addition to its application in metal protection and its common use in coating technology, hopeite is also one of the main crystalline reaction products of dental cement[15,16] and has lead to a new generation of dental ceramic formulations: the zinc phosphate cements (ZPC).[17–19] Active research has recently been conducted in dental medicine to obtain materials suitable for fabrication of aesthetic single crowns or fixed partial dentures for permanent restoration of teeth.[20,21] Zinc phosphate based cements or glass ionomer/phosphate cements generally perform well because of high fracture toughness,[22,23] low solubility in an aggressive biological environment[24] and high bonding strength with any other adhesive cement or with bone substrate conferring good chemical stability, durability and low cytotoxicity, that is, excellent biocompatibility. However, long-term clinical studies comparing different dental materials show that optimisation of the elastic-modulus/fracture-toughness relationship and a dramatic lowering of the solubility are still necessary.[25–27]

Since the first microporous zinc phosphates with zeolite-like topologies were reported by Gier and Stucky,[28] a large number of zincophosphates (ZnPOs) with one-, two- and three-dimensional structures have been synthesised in the presence of organic templates.[29,30] Although several hypotheses have been suggested, the mechanism of formation of complex two- and three-dimensional open framework structures is still poorly understood. However, hopeite is believed to be one of the precursors of zinc phosphate based zeolites, as it is gradually transformed into ladderlike and layered

[a] L. Herschke, Dr. V. Enkelmann, Dr. I. Lieberwirth, Prof. Dr. G. Wegner
Max-Planck-Institute for Polymer Research
Ackermannweg 10, 55128 Mainz (Germany)
Fax: (+49) 6131-379-100
E-mail: lieberw@mpip-mainz.mpg.de

 DOI: 10.1002/chem.200305693 © 2004 Wiley-VCH Verlag GmbH & Co. KGaA, Weinheim

three-dimensional structures by substantial incorporation of the respective template agent, thus involving significant hydrogen bonding.[31,32]

All these materials which are geared towards advanced applications share the feature that, as far as synthesis and purity are concerned, the nature of the zinc phosphate hydrate (α- or β-hopeite, parahopeite or $Zn_3(HPO_4)_3{\cdot}3H_2O$ (ZHPT)) has a dramatic influence on pigment activation,[33–35] bioactivity[36,37] and the resulting macrostructure.

In nature zinc phosphate tetrahydrate exists in two structures, orthorhombic hopeite and parahopeite, its triclinic polymorph. Although the phase system P_2O_5–ZnO–H_2O had been studied for a very long time,[38,39] the precise structure of the two orthorhombic modifications, α- and β-hopeite, was not previously known.

This work is focused on the systematic identification of the two polymorphs of zinc phosphate tetrahydrate, their comparison with the precursor $Zn_3(HPO_4)_3{\cdot}3H_2O$ and refinement of their crystal structures,[40] allowing a direct correlation between structure and properties. α-Hopeite is considered the most stable polymorphic form and β-hopeite is a comparatively metastable form obtained at lower temperature (20 °C). Careful identification of the hydrogen-bonding network in the different forms of zinc phosphate is expected to offer a starting point for future efficient modifications of zinc phosphate based materials such as dental cements, catalysts based on zeolite technology and "green" anticorrosion inhibitors.

Experimental Section

α,β-Zinc phosphate tetrahydrate (ZPT) macrocrystals: A buffered solution of concentrated phosphoric acid (100 mL) was prepared by slowly adding solution of ammonia in water (Riedel–de Haën, 25 wt% solution diluted × 10, 27 mL) to phosphoric acid (Aldrich, ACS grade, 85 wt% solution diluted × 4, 73 mL), so that H_3PO_4 (50 mol%) reacted with ammonia to give a solution of ammonium hydrogen phosphate (0.792 mol L^{-1}) in water. The mixture was stirred vigorously for 2 h at 0 °C. Another solution (0.114 mol L^{-1}) prepared from zinc acetate (Aldrich, ACS grade, 5 g) and water (Millipore grade, 18.6 MΩ cm^{-1}, 100 mL) was transferred into a sealed crystallisation reactor and kept there for 2 h at 90.0 °C (±0.1 °C) under reflux under an inert gas atmosphere (argon). The partially neutralised phosphate solution (30 mL) was added to achieve the molar ratio $Zn/PO_4/NH_4 = 1:1.05:0.52$. The white precipitate that formed redissolved quickly as the pH reached 1.45, during which the solution was stirred at 1250 rpm. An NaOH solution (pellets, Riedel–de Haën, ACS grade, 4 mol L^{-1}) was added dropwise to the reaction mixture over a period of five days, without stirring, to yield a white precipitate. After two days of ageing, the first transparent crystals of hopeite appeared at the precipitation front/solution interface, corresponding to a slow change in pH from 1.5 to approximately 2.6. Further addition of NaOH gave rise to slowly growing α-hopeite crystals. At pH 6 the reaction was stopped and crystals of the product were recovered from their mother liquor by filtration, washed to neutral pH and dried at room temperature for 12 h.

β-Zinc phosphate tetrahydrate (commonly designated as β-hopeite or β-ZPT) crystals were obtained by the same procedure with a zinc acetate solution (57 mmol L^{-1}). The crystallisation temperature was fixed at 20.0 ± 0.1 °C.

α,β-Zinc phosphate tetrahydrate (ZPT) crystalline powders: The synthesis described above yielded α- and β-hopeite macrocrystals, which were then used for single-crystal determination. All other analyses were performed using a well dried crystal powder obtained by mixing a solution of zinc acetate in water (Aldrich, ACS grade, 100 mL, 0.114 mol L^{-1}) with phosphoric acid (Aldrich, ACS grade, 85 wt% solution diluted × 4, 5.5 mL) for two hours at pH 4 with gentle stirring at 90.0 and 20.0 °C for α- and β-ZPT, respectively.

Zinc hydrogen phosphate trihydrate macrocrystals: Large crystals of zinc hydrogen phosphate trihydrate (ZHPT) could be obtained by slightly changing the α-hopeite synthesis procedure described above. A buffered solution of concentrated phosphoric acid 100 mL (6.13 mol L^{-1}) was prepared as for the α-hopeite synthesis, but with neutralisation of up to 70 mol% of H_3PO_4 with ammonia. A solution of zinc acetate in water (150 mL, 2.5 mol L^{-1}) was stored in a sealed crystallisation reactor for 2 h at 90.0 °C to achieve thermal equilibrium. After adding successively the phosphate solution (62.5 mL) and a 5 M nitric acid solution (Riedel–de Haën, 65 wt% solution, 6.13 mol L^{-1}), a pH of 0.25 was reached. When 5 M NaOH (37 mL) was added dropwise over two days, flat needle-shaped ZHPT crystals formed. For mass-transfer crystal (diffusion-dependent) growth of $Zn_3(HPO_4)_3{\cdot}3H_2O$ crystals up to millimetre size, triethanolamine (Aldrich, 98 wt%, only 3 mL) had to be added to the reaction medium.[41]

Characterisation: Elemental analysis of the precipitate was conducted by atomic absorption spectroscopy (Perkin–Elmer PE5100ZL with a Zeeman Furnace Module and AS70 sampler) and by colorimetric phosphate titration (blue molybdate complexometric method) using UV/Vis spectrometry (Perkin–Elmer Lambda 900).[42] The estimated standard deviation from the stoichiometric composition was ±0.04. pH values were measured with a Pt/KCl glass electrode attached to a pH meter (Schott CG843 set) with an integrated temperature sensor (Blueline 14pH, Schott). Before the measurements, the pH electrode was calibrated with three buffer solutions at pH 4.006, 6.865 and 9.180 at 20.0 °C (DIN Norm 19266). DSC measurements were performed under a nitrogen atmosphere on a Mettler–Toledo DSC30S module with a TC15 TA controller; heating rate: 10 °C min^{-1}, heating range: 0–500 °C). Similarly TGA-MS curves were obtained under an argon atmosphere on a Mettler–Toledo ThermoSTAR® TGA/SDTA851 equipped with a Pfeiffer Vacuum GSD 300T2 pump and a Balser MS/Netsch STA449C mass detector (heating rate: 10 °C min^{-1}, heating range 0–600 °C).

Scanning electron micrographs were taken with a Leo Gemini 1530 operated at 1 kV from a 35° angle side detector at a working distance of 5 mm.

DRIFT (diffuse reflectance infrared Fourier transform) spectra were recorded with a Nicolet 730 spectrometer (liquid N_2-cooled MCT detector) on powder samples (10 wt% sample, 90 wt% KBr, total amount 300 mg). Background and spectra were collected with a nominal resolution of 4 cm^{-1}, double averaging over 128 scans in the frequency range 400–4000 cm^{-1}.

Powder X-ray data for an as-synthesised sample of crystals (placed on a 2 cm circular silicon monocrystal slide) were collected at 25 °C on a Seifert XRD3000TT Bragg–Brentano diffractometer with a linear, position-sensitive detector (5° 2θ) in Debye–Soller geometry with a flat secondary monochromator and employing Ge monochromated $Cu_{K\alpha_1}$ radiation (λ = 1.5406 Å). For structure determination of the three zinc phosphate polymorphs (single-crystal diffraction method), a suitable crystal with dimensions 100 × 50 × 50 μm^{-3} was used. Data collection for the crystal structure analyses was performed on a Nonius KCCD diffractometer with graphite monochromated $Mo_{K\alpha}$ radiation (λ = 0.71073 Å). The structures were solved by direct methods. They were refined by full-matrix least-squares analyses on F^2 with anisotropic temperature factors for the non-hydrogen atoms. The hydrogen atoms were located in difference Fourier maps and refined isotropically in the riding mode. Pertinent crystallographic data are summarised in Table 1. CCDC-413637 (α-hopeite), CCDC-413638 (β-hopeite), and CCDC-413639 ($Zn_3(HPO_4)_3{\cdot}3H_2O$) contain the supplementary crystallographic data for this paper. These data can be obtained free of charge via www.ccdc.cam.ac.uk/conts/retrieving.html, or from the Cambridge Crystallographic Data Centre, 12 Union Road, Cambridge CB21EZ, UK; fax: (+44) 1223-336033; or email: deposit@ccdc.cam.ac.uk.

© 2004 Wiley-VCH Verlag GmbH & Co. KGaA, Weinheim

Table 1. Lattice parameters, data collection and structure refinement of hopeite polymorphs and their precursor $ZnHPO_4 \cdot H_2O$.[a]

	α-Hopeite[b]	α-Hopeite	β-Hopeite	$ZnHPO_4 \cdot H_2O$
crystal data				
formula	$Zn_3(PO_4)_2 \cdot 4H_2O$	$Zn_3(PO_4)_2 \cdot 4H_2O$	$Zn_3(PO_4)_2 \cdot 4H_2O$	$Zn_3(HPO_4)_3 \cdot 3H_2O$
M_r [g mol^{-1}]	458.11	458.11	458.11	538.08
T [K]	290	230	290	290
crystal system	orthorhombic	orthorhombic	orthorhombic	triclinic
space group	*Pnma*	*Pbnm*	*Pbnm*	$P\bar{1}$
a [Å]	10.629	5.0135(3)	5.0266(2)	8.4746(4)
b [Å]	18.339	10.6044(5)	10.6060(4)	9.8688(5)
c [Å]	5.040	18.2828(7)	18.2946(5)	9.8895(5)
α [°]	90.0	90.0	90.0	112.0618(13)
β [°]	90.0	90.0	90.0	111.9702(13)
γ [°]	90.0	90.0	90.0	96.9953(12)
V [Å^3]	982.4	972.0(1)	975.3(1)	676.9(1)
Z	8	8	8	2
ρ_{calcd} [g cm^{-3}]	3.096	3.1301	3.1223	2.6396
refinement				
reflections measured	1471	16792	11249	8100
independent reflections	1415	1582	1369	3535
refined parameters	–	85	85	187
reflections observed [$I > 3\sigma(F^2)$]	1415	857	857	2514
R_{int}	0.064	0.065	0.041	0.0025
R	0.064	0.0277	0.0290	0.0492
R_w	0.068	0.0384	0.0327	0.0523
GOF	–	1.068	1.368	1.011

[a] Calculated standard deviations are in parentheses. [b] Reference [63].

Results and Discussion

Analysis of samples and crystal morphology:

Electron microscopy: The α-hopeite crystals used in this study (Figure 1a) possessed the classical plate shape and are reasonably uniform in size (about $1000 \times 250 \times 0.5\ \mu m^3$), whereas β-hopeite crystals (Figure 1c) were not as well defined; they were slightly smaller and partially agglomerated. The development of the faces of α-hopeite crystals is sometimes irregular and the crystals may simulate disphenoidal or hemimorphic symmetry. The β-hopeite sample has two different habits: tabular {010} and prismatic {001}. This platelike habitus of hopeite crystals corresponds to a layered structure, the *b* axis being the crystal-plate normal.[43] The zinc hydrogen phosphate trihydrate crystals (Figure 1e,f) are found as elongated {001} and tabular {100} plates of vitreous appearance and cleaved {010} planes.

Phase composition: From elemental analysis and thermogravimetry data, the calculated exact stochiometric compositions were : α-hopeite, $Zn_{2.92}(PO_4)_{1.95} \cdot 3.98 H_2O$; β-hopeite, $Zn_{2.95}(PO_4)_{1.90} \cdot 3.96 H_2O$; ZHPT, $Zn_3(HPO_4)_3 \cdot 2.99 H_2O$. In the cases of α- and β-hopeite all these values match nearly perfectly with the zinc phosphate tetrahydrate stochiometry. Seemingly phosphate incorporation into the crystal structure of β-hopeite is facilitated at 20.0 °C, in comparison with 90.0 °C, because of the preferential decomposition of $Zn(HPO_4)_3 \cdot 3H_2O$ and also $ZnHPO_4 \cdot 3H_2O$ at pH 4 and 20.0 °C in the liquid phase; this explains the tiny differences in stoichiometry between the two polymorphs. Similarly Salmon and Terrey's results could suggest that the formation of α-hopeite at 90.0 °C results from the decomposition of a metastable zinc monohydrogen phosphate monohydrate and trihydrate [Eq. (1)].[44]

$$\begin{aligned} &Zn(H_2PO_4)_2 \cdot 2H_2O \rightarrow Zn_3(HPO_4)_3 \cdot 3H_2O \rightarrow \\ &ZnHPO_4 \cdot H_2O \rightarrow ZnHPO_4 \cdot 3H_2O \rightarrow \\ &Zn_3(PO_4)_2 \cdot 4H_2O \end{aligned} \quad (1)$$

Powder diffraction: All the specimens were examined by X-ray powder diffraction[45] and also to validate the method of synthesis. The two main polymorphs of the tetrahydrate (α- and β-hopeite) are not distinguishable by XRD (Figure 2a,b). It may be concluded that the non-hydrogen atom positions within the crystal structures are essentially identical. Therefore, methods of differentiation between α- and β-hopeite are required to distinguish clearly between the hydrogen bonding in the polymorphs, that is, DRIFT measurements and thermogravimetry.

DRIFT measurements: DRIFT (Figure 3) allows sensitive and fast detection of the two forms of zinc phosphate tetrahydrate. The symmetry of a "free" PO_4^{3-} ion is T_d and the nine modes of internal vibrations span the representation $\Gamma_{vibr}(T_d) = A_1 + E + 2F_2$.[46,47] Here A_1 represents the symmetric stretching mode ν_s(P–O) located at $\approx 980\ cm^{-1}$, E represents the symmetric bending mode δ_s(OPO) at $\approx 420\ cm^{-1}$, and the triply degenerate modes F_2 represent the antisymmetric bending mode δ_{as}(OPO), located at $\approx 560\ cm^{-1}$. However, there are slight shifts from the known spectra of α-hopeite due to solid-state effects and specificities of the DRIFT technique.[48] In Figure 3, below $1200\ cm^{-1}$ (phosphate region), α- and β-hopeite show very similar spectra, confirming the uniformity of the non-hydrogen framework. The bands observed at 1102–1005, 945–928,

 © 2004 Wiley-VCH Verlag GmbH & Co. KGaA, Weinheim

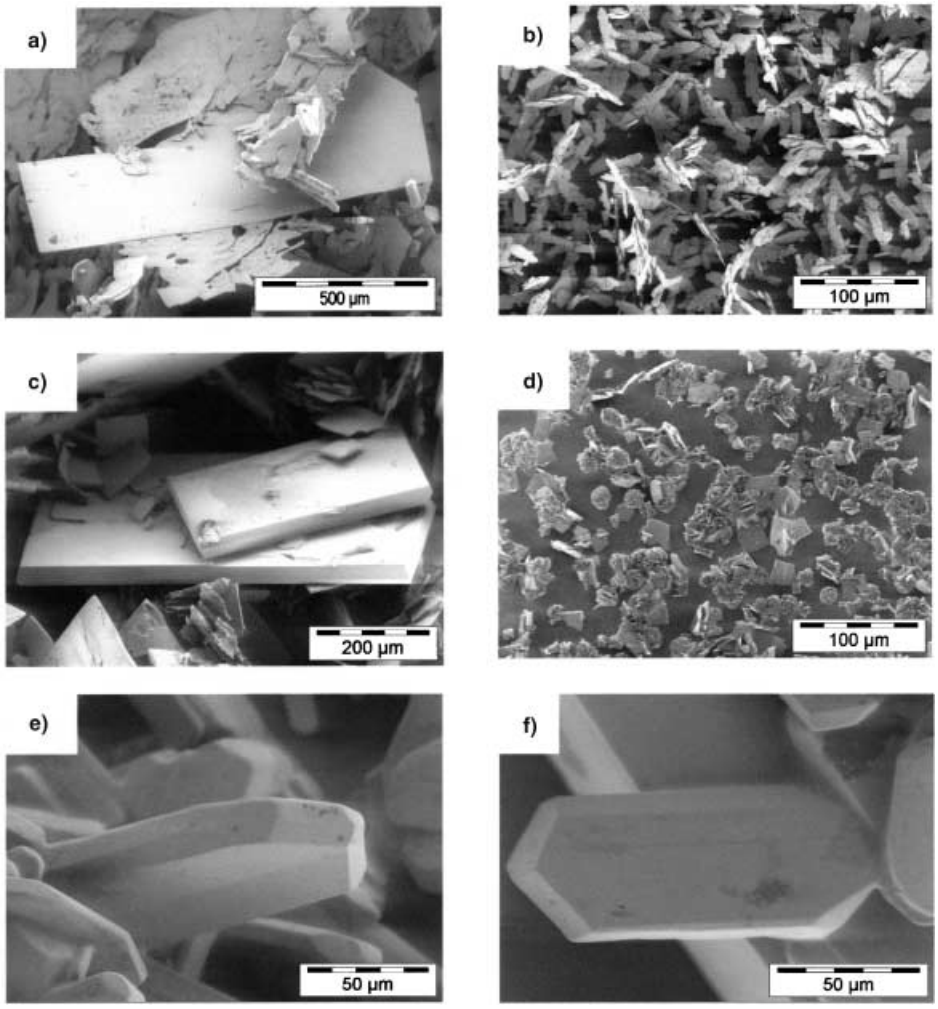

Figure 1. SEM images: Crystals suitable for single-crystal analysis: a) α-hopeite; c) β-hopeite; e, f) $Zn_3(HPO_4)_3{\cdot}3H_2O$. Samples suitable for X-ray powder diffraction: b) α-hopeite; d) β-hopeite.

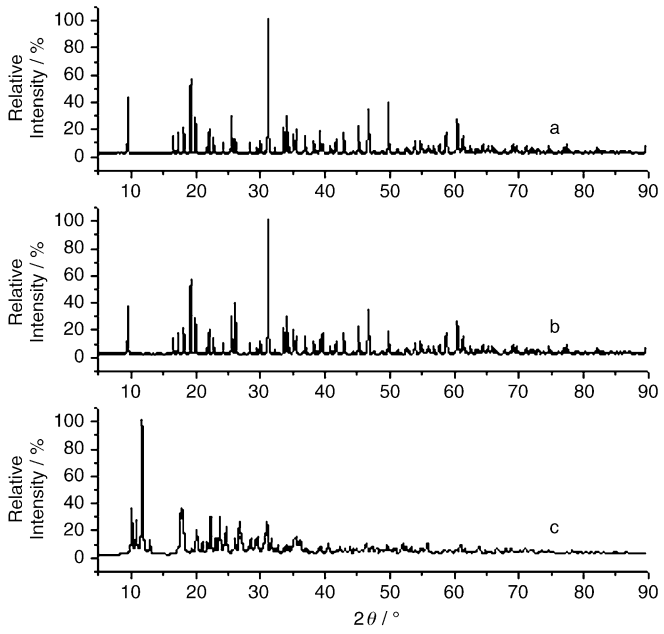

Figure 2. X-ray powder patterns of a) α-Hopeite; b) β-hopeite; c) $Zn_3(HPO_4)_3{\cdot}3H_2O$.

635–584 and 414 cm^{-1} (the last band is not shown in Figure 3) are assigned to $\nu_{as}(P{-}O)(\nu_3)$, $\nu_s(P{-}O)(\nu_1)$, $\delta_{as}(OPO)(\nu_4)$ and $\delta_s(OPO)(\nu_2)$, respectively. In comparison with α-hopeite (orthorhombic) the ν_1 mode of the intermediary compound (ZHPT) is stronger, sharper and shifted to 911 cm^{-1}, indicating a more open or distorted sphere of coordination of phosphate groups.[49,50] Multiple ν_3 vibrations in the region between 1220 and 1123 cm^{-1} indicate that the zinc hydrogen phosphate trihydrate belongs to a less ordered space group (triclinic).

The "free" H_2O group has three modes of internal vibration occurring at frequencies 3765, 3652 and 1640 cm^{-1}.[51] The large peak around 1640 cm^{-1} in the α-hopeite spectrum corresponds to the internal bending (ν_3) vibration of crystal water molecules, while the broad, very strong band centred around 3300 cm^{-1} represents stretching (ν_1 and ν_3) modes, shifted to lower frequencies from their ideal value because of hydrogen bonding. The band at 1639 cm^{-1} is broader in the spectrum of β-hopeite than in that of the α form. The

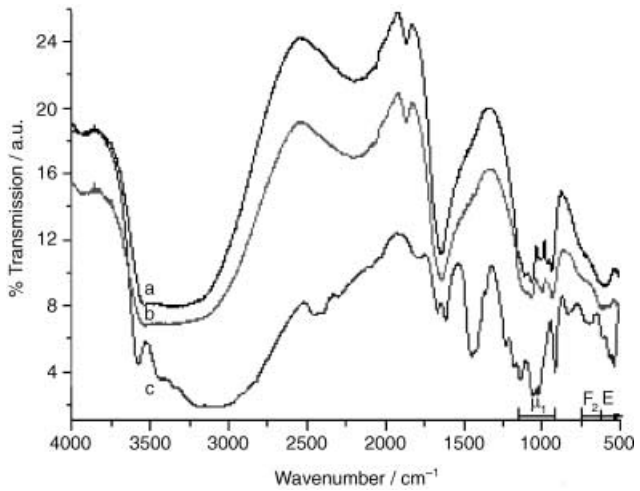

Figure 3. Comparison of DRIFT spectra of the two polymorphs of zinc phosphate tetrahydrates, a) α-hopeite and b) β-hopeite, and of a precursor compound, c) $Zn_3(HPO_4)_3{\cdot}3H_2O$.

© 2004 Wiley-VCH Verlag GmbH & Co. KGaA, Weinheim

shape of the H_2O stretching region of ZHPT is significantly different from those of α- and β-hopeite, with a decoupling of bands at 1601 and 1673 cm^{-1} indicating at least two types of water molecules.[52] In addition, the ZHPT form presents a strong peak at 3580 cm^{-1}, constituting additional evidence for the variability of hydrogen-bonding schemes within the framework of the two polymorphs of zinc phosphate tetrahydrate and its precursors.

Thermoanalysis: Both orthorhombic modifications of $Zn_3(PO_4)_2{\cdot}4H_2O$ show dehydration starting above 100 °C and appearing to be complete at about 400 °C (Figures 4 and 5). The thermogravimetric (TGA-MS) curves demonstrate the characteristic behaviour of α-hopeite: it loses crystal water in two well-defined stages, two molecules at 146 °C and the remaining two at 330 °C. Similarly the DSC measurement gives two well-separated but slightly displaced peaks: a sharp peak at 182 °C and a "double" peak at 278 and 298 °C, which may indicate the starting point for the loss of two types of water molecule. At about 220 °C, that is, after loss of 2.02 H_2O, a pseudo-stabilisation of the structure is reached; the water loss increases slowly, indicating the existence of a dihydrate structure. These results confirm that the first step corresponds to the tetrahydrate–dihydrate transition, and the second step to the dihydrate–anhydrate transition.[53,54]

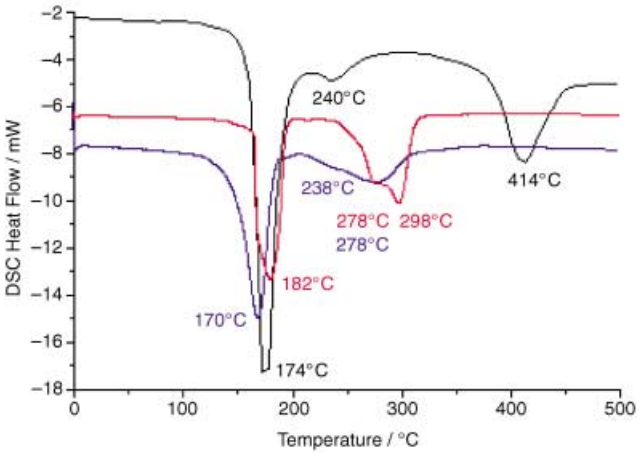

Figure 4. DSC curves of α-hopeite (red), β-hopeite (blue) and $Zn_3(HPO_4)_2{\cdot}3H_2O$ (black). Heating rate $q = 10\,°C\,min^{-1}$.

The thermograms of β-hopeite show significant differences from the α phase. β-Hopeite seems to have a lower activation energy of dehydration than the α-hopeite, pointing towards a lower symmetry of the four water molecules contained in the crystal. This is confirmed by DSC: the onset thermal decomposition appears at 115 °C for the β form and 130 °C for the α form. Whilst no gradation is clearly observable on the TGA weight loss curve of β-hopeite between the dihydrate and the anhydrous salt, the DSC curve (Figure 4, blue line) presents two peaks at 238 and 278 °C, and there is a shoulder on the TGA curve at a water content corresponding to the monohydrate.[55] Surprisingly, this transition at 238 °C also corresponds to the temperature at which the dihydrate is formed from α-$Zn_3(PO_4)_2{\cdot}4H_2O$. Thus, we observe the loss of two water molecules in the transformation from dihydrate to anhydrous salt, but the transformation from β-hopeite to "β-dihydrate" is different. In this last case, a shoulder appears in both the TGA-MS and DSC curves at 130 °C that may be attributed to the formation of

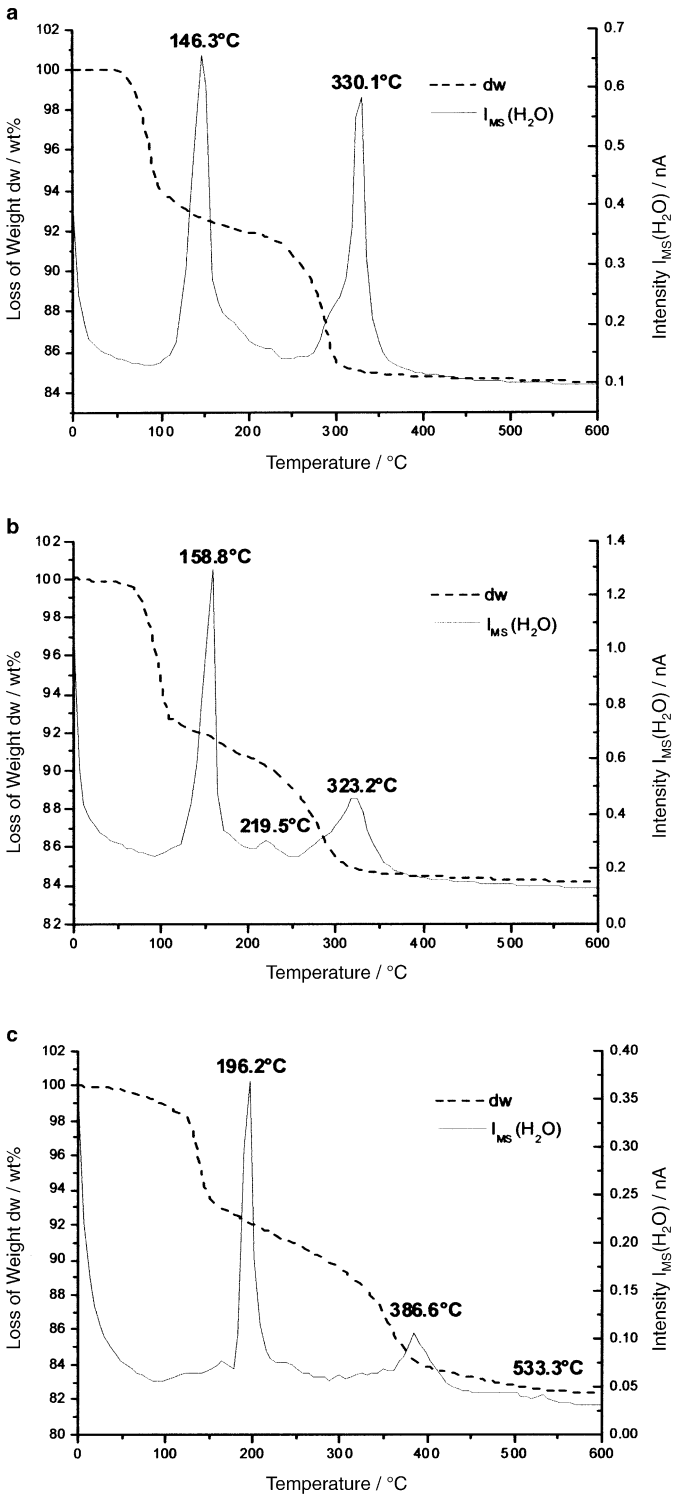

Figure 5. Typical TGA-MS curves of: a) α-hopeite; b) β-hopeite; c) $Zn_3(HPO_4)_2{\cdot}3H_2O$. Heating rate = 10 $K\,min^{-1}$ with 25 mg of sample.

 © 2004 Wiley-VCH Verlag GmbH & Co. KGaA, Weinheim

an unstable trihydrate. A broad endothermic peak detected by DSC at 170 °C accompanies the removal of 1.69 water molecules.[56] In summary, the β-hopeite loses its four water molecules one after another in four consecutive steps. These results are in partial disagreement with the thermal behaviour of β-hopeite previously reported in the literature.[57] Furthermore, under the present heating conditions, the eventual β→α-hopeite transition does not occur before the beginning of dehydration, as very different dehydration pathways are observed above 130 °C. It is therefore concluded that the kinetics of a β→α-hopeite transition must be very slow.

For the last compound (ZHPT), the dehydration process is also notably different from that of α-hopeite: after a non-uniform dehydration between 100 and 220 °C, corresponding to the loss of 0.99 water molecules, successive peaks occur at 386 and 533 °C, corresponding to the loss of 1.53 and 0.47 H_2O molecules, respectively. However DSC data exhibit two peaks at 174 and 240 °C related to the formation of a dihydrate, and a further single dehydration peak at 414 °C. This thermal anomaly, similar to that observed for β-hopeite at 238 °C but at a higher temperature, may be interpreted by the intermediate formation of a compound whose water content varies from dihydrate (α,β-form: 214 °C) and from monohydrate (α,β-form: 286 °C)[58] or by the transformation of the monohydrogen phosphate group to a phosphate group.[59]

From all these analyses, it may be concluded that the non-hydrogen atom positions within the crystal structures are essentially identical (DRIFT) and therefore the marked difference in thermal response of the two polymorphs of zinc phosphate tetrahydrate primarily involves changes in hydrogen bonding pattern alone.[60,61] Furthermore, these last observations are supported by the differences in thermodynamic stability measured by Gardner and co-workers for α- and β-hopeite.[62]

Structure description: The structure of α-hopeite was reported previously[40,63,64] but not described completely because of the missing hydrogen atom locations. Early descriptions of an epitaxial growth of the β-phase of zinc phosphate tetrahydrates on a zinc crystal were given by Omori and Okabe,[65] who reported similar values of lattice parameters to those found by Gamidov and Galovachev.[66] However, no previous studies could distinguish the α form from the β form of zinc phosphate tetrahydrate crystallographically.

The crystal structure of many minerals can be understood through a representation of the framework of coordination polyhedra in which the structural similarities of a group of related structures can be made visible. Thus in a number of quite different compounds, for example, in the family of apatites and hydroxyapatites,[67] crystal structures can be derived from one aristotype and the crystal chemistry can be systematised as variations of one common structural principle. In apatites the wealth of different structures also arises from the possibility of nonstoichiometric compositions. This is not the case with the zinc phosphates studied here. There is no experimental evidence for deviations from the integral stoichiometries. The crystallographic data for α- and β-hopeite and ZHPT, and a comparison with reliable reference data for the α-form, are given in Table 1.

The crystal structures of zinc phosphates can be described in terms of a framework built from ZnO_6 octahedra, ZnO_4 tetrahedra and PO_4 tetrahedra. The other known hydration states[68,69] and zinc hydrogen phosphates can be understood by using this approach. Two projections of the hopeite structure in the planes *ac* and *bc* are shown in Figure 6. In this

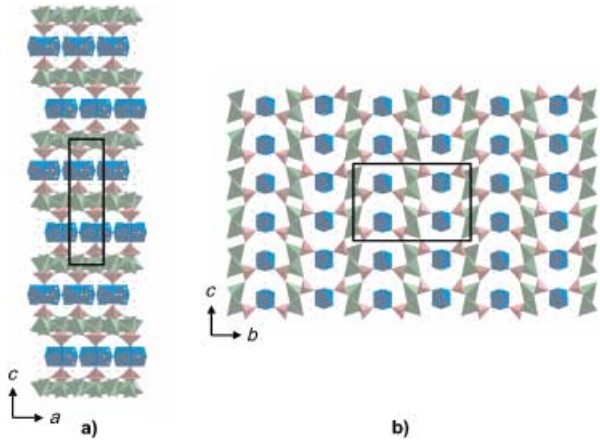

Figure 6. Sheet arrangement of Zn^{II}-centred polyhedra and phosphate tetrahedra in zinc phosphate tetrahydrate. The framework is identical for α- and β-hopeite. The connectivity is emphasised in projections along a) [010] and b) [100]. The green and magenta tetrahedra describe ZnO_4 (coodination 4) and PO_4 groups respectively. The blue octahedra symbolise the ZnO_6 (coordination 6) groups.

structure ZnO_6 octahedra contain the four water molecules. The remaining two oxygen atoms share corners with two PO_4 tetrahedra. These share corners with two ZnO_4 tetrahedra and an edge with a third. The hopeite structure can thus be characterised as a layer structure in which layers of the closely connected PO_4 and ZnO_4 tetrahedra are separated by ZnO_6 octahedra. Alternatively the structure of hopeite can be described as tetrahedral sheets of zigzag chains of corner-sharing ZnO_4 moieties connected by shared corners with PO_4 and thus with ZnO_6 to produce a complex sheet of three- and four-membered rings. This layer character is clearly visible in the *ac* projection (Figure 6b). The connection between the layers is comparatively weak; with the exception of the corner-sharing oxygen atoms mentioned above, it is formed by hydrogen bonds. The main cleavage plane of hopeite crystals is found to be parallel to this interface. However, this interface contains no voids that could be used to include additional atoms or ions. The high packing density of hopeite is also reflected by the high crystal density.[70]

Unlike the case of the above-mentioned apatites, in zinc phosphates hydrogen bonds play a dominant role in the packing and crystal chemistry. In α- and β-hopeite all non-hydrogen atoms are found in identical positions. This leads to the surprising result that the two forms, which exhibit markedly different thermal behaviour, differ only in the position of a few hydrogen atoms, that is, in the orientation in which water molecules are coordinated in the ZnO_6 octahe-

© 2004 Wiley-VCH Verlag GmbH & Co. KGaA, Weinheim

dra. The different water orientations give rise to different hydrogen-bonding patterns. We were able to locate all the hydrogen atoms in the α- and β-hopeite structures in the difference Fourier maps.

The crystal structures of α- and β-hopeite are shown in Figure 7. In the β form the two water molecules located on the mirror plane (O8 and O9, respectively) are oriented so that the molecular plane coincides with the mirror plane. In α-hopeite one of these (O8) is oriented perpendicular to the mirror plane. In this orientation a strong intra-octahedron hydrogen bond is formed that may account for the higher thermal stability of the α form. The other hydrogen bonds are inter-octahedron or to neighbouring ZnO_4 or PO_4 tetrahedra, and do not differ significantly in the two crystal forms. Comparison of hydrogen-bonding geometry, including bond lengths and contact angles, is given in Table 2; hydrogen atoms are labelled as in Figure 8. For α- and β-hopeite, the distances and angles involved in both hydrogen bonding schemes lie well within the accepted range of hydrogen bond lengths,[71] whereas the interatomic (donor–acceptor) distances for O9–O6 (α-hopeite) and O8–O10 (β-hopeite) are near the end of the range (2.2–3.1 Å). Corrected values for hydrogen bonds are higher than those obtained by Whitaker for α-hopeite[63] (1.719 versus 1.54 Å for the shortest length), because of thermal distortion effects. Although the angles subtended by the hydrogen atom at the water oxygen atom fluctuate noticeably between 45° and 90° for β-hopeite and between 90° and 110° with a maximum at 108.34° for α-hopeite, both geometries are nearly tetrahedral. It was found that the hydrogen bonds were never collinear in α-hopeite so that the hydrogen atoms subtended an angle of 109° at the donor oxygen although the acceptors did not. However, in view of the O9–H9-1–O10 angle (179.88°) existing uniquely in the α-

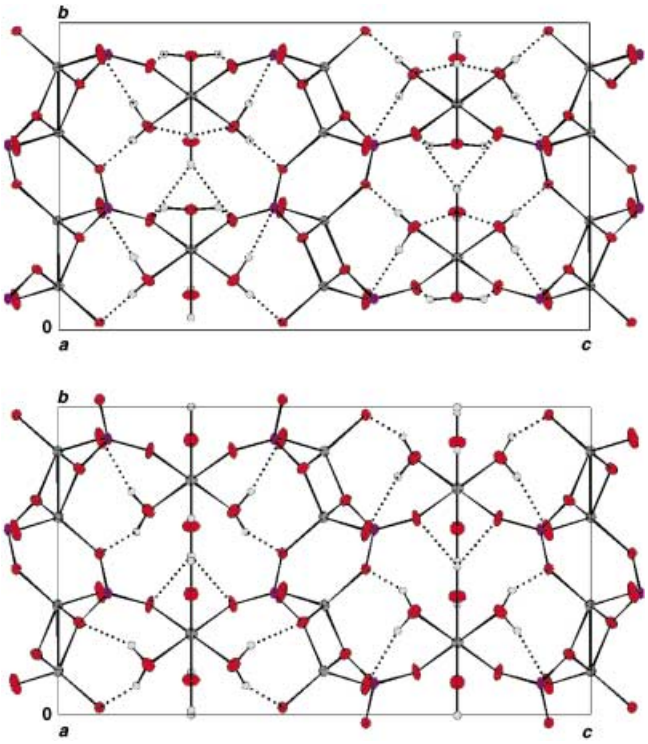

Figure 7. Unit cells of the α-$Zn_3(PO_4)_2{\cdot}4H_2O$ (top) and β-$Zn_3(PO_4)_2{\cdot}4H_2O$ (bottom) structures are shown in projection onto the *bc* plane (50% thermal displacement ellipsoids). The Zn cations are shown in dark grey, the P atoms in violet, the O atoms in red and the H atoms in light grey. Broken lines represent hydrogen bonds.

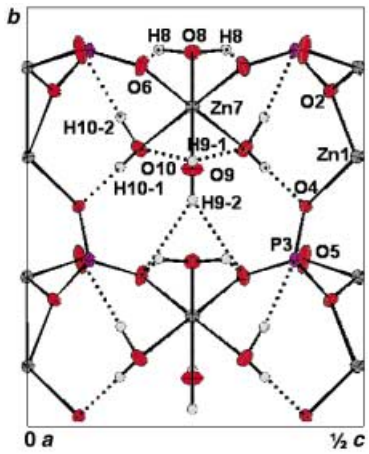

Figure 8. Projection of half of the asymmetric unit cell along the *a* axis, valid for both α- and β-zinc phosphate tetrahydrate.

Table 2. Distances and angles involved in hydrogen bonds for α- and β-hopeite.[a]

Hydrogen bonding			Distance [Å]			Angle [°]		
Donor O_a(water)	H_i	Receptor $O_b(PO_4)$	O_a–O_b	O_a–H	H–O_b	O_b-O_a-O_b*	O_a-H-O_b	H-O_a-H
α-hopeite								
O8	H8	O6	2.78	0.79	1.72	148	113	100
O10	H10-1	O4	2.71	0.87	1.83	72	58	108[b]
O10	H10-2	O5	3.02	0.95	2.07	82[e]	180	92
O9	H9-1	O10	2.89	0.75	2.23	116[c]	39	108[b]
O9	H9-2	O8	3.06	1.21	2.45	32[c]		
	124	108[d]						
O9	H9-2	O6	3.12	0.79	2.45	49[c]	142	108[b,d]
β-hopeite[f]								
O10	H10-1	O2	2.71	0.99	1.78	104	155	47
O10	H10-2	O5	3.02	0.89	2.14	74	169	60[g]
O9	H9-2	O6	3.12	1.10	2.20	60	139	73
O8	H8	O10	3.22	1.14	2.34	51	135	82

[a] Estimated standard deviations: ±0.01 Å for lengths; ±0.5° for angles. [b] For the angle H10-1–O10–H10-2. [c] For the angle with O_b*, symmetrical to O_b through the *ac* mirror plane. Other angles were obtained using *bc* as the mirror plane. [d] For H9-2–O9–H8 the angle is 56°. [e] Observing O5 as symmetric with O5 through the *ac* plane, the angle is 60.49° for O5–O9–O5. [f] All angles are measured with O_b*, symmetric with O_b through the *bc* mirror plane. [g] For the angle H10-2–O10–H10-1, the measured value is 100°.

 © 2004 Wiley-VCH Verlag GmbH & Co. KGaA, Weinheim

ZPT, substantial structural stabilisation is achieved by the assured contact between zinc octahedra and tetrahedra.

A projection of the crystal structure of ZHPT is shown in Figure 9. The sheet structure consists of ZnO_6 octahedra, which are located on symmetry centres and contain four water molecules. The remaining two oxygen atoms share a

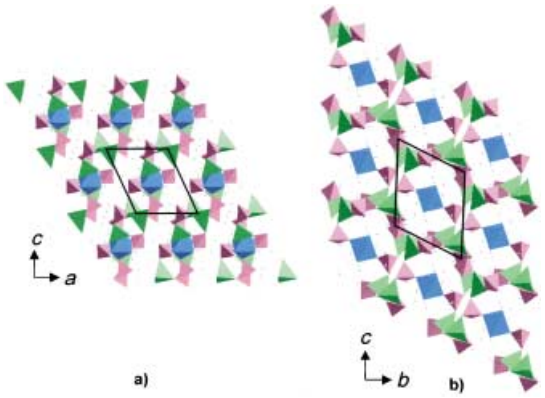

Figure 9. Sheet arrangement of Zn^{II}-centred polyhedra and phosphate tetrahedra in zinc hydrogen phosphate trihydrate (ZHPT). The connectivity is emphasised in projections along a) [010] and b) [100]. The green and magenta tetrahedra describe ZnO_4 (coodination 4) and PO_4 groups respectively. The blue octahedra symbolise the ZnO_6 (coordination 6) groups.

corner with PO_4 tetrahedra. Three of the oxygen atoms of the PO_3OH groups share a corner with ZnO_4 tetrahedra. This network geometry of Zn–PO_4 bonding (continuous six-ring channels) clearly has some similarities with other compounds of the ZnO–P_2O_7–H_2O system such as parahopeite.[72,73] This arrangement of cation-centred polyhedra and phosphate tetrahedra is emphasised in Figure 9a,b. The structure contains one additional water molecule that is not coordinated to zinc. All water molecules and OH groups take part in hydrogen bonds, creating a three-dimensional network, which for clarity is not shown in Figure 10 but can easily explain the high dehydration temperatures documented in the DSC thermogram.

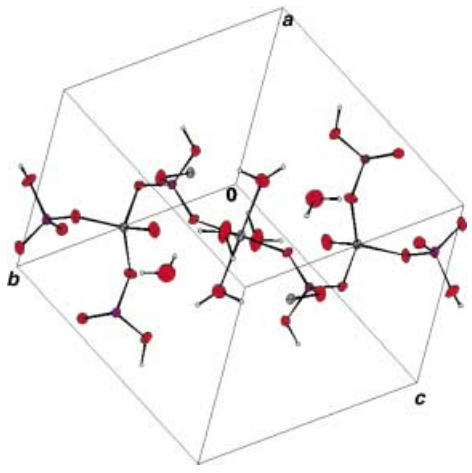

Figure 10. Unit cell of $Zn_3(HPO_4)_3{\cdot}3H_2O$ (with 50% thermal probability ellipsoids). The inversion centre of symmetry passes through the octahedrally coordinated zinc. The Zn cations are shown in dark grey, the P atoms in violet, the O atoms in red and the H atoms in light grey.

Conclusion

We have demonstrated a new, simple method of synthesizing macrocrystals of two zinc phosphate tetrahydrates: α- and β-hopeite. XRD proves that the non-hydrogen atom positions within the crystal structures are essentially identical. However, differentiation of the two phases becomes possible by using thermoanalysis and DRIFT. The marked difference in thermal response primarily involves changes in hydrogen-bonding alone. Single-crystal analysis proves that the main difference between the α- and β-forms of zinc phosphate tetrahydrate is caused by the orientation of one of the water molecules in the ZnO_6 octahedra. Whereas in β-hopeite two water molecules (O8 and O9) are located on the mirror plane and are oriented so that the molecular plane coincides with the mirror plane, in α-hopeite one of these (O(8)) is oriented perpendicular to the mirror plane. Further, the zinc hydrogen phosphate trihydrate (ZHPT) structure shows striking similarities to another zinc phosphate tetrahydrate, parahopeite. The analysis and understanding of the role of hydrogen bonding in these seemingly simple zinc phosphate structures give a better appreciation of the interaction mechanisms of proteins with more complex structures of biological interest, such as hydroxyapatite. Hopeite has great potential as a starting material for various applications, such as development of advanced formulations of anticorrosive pigments by careful substitution of zinc with other divalent metal atoms, or synthesis of large-open framework zeolitic structures used for enantioselective separation by acting as a source of zinc and phosphate ions.

Acknowledgement

The authors thank the Bundesministerium für Bildung und Forschung (the German Ministry for Education and Research, BMBF) for financial support of this work under the project "Water as a medium for synthesis, transformations and applications of plastics", and also BASF AG. Special thanks are extended to Dr. B. Mathiasch and Dr. H. W. Werner from the Johannes Gutenberg Universität Mainz for their expertise and helpful discussions concerning analytical problems.

[1] D. Darling, R. Rakshpal, *Mater. Perform.* **1998**, *37*, 42.
[2] I. M. Zin. S. B. Lyon, S. J. Badger, J. D. Scantlebury, V. I. Pokhmurskii, *J. Corros. Sci. Eng.* **1999**, *2*, 21.
[3] L. Veleva, J. Chin, B. Del Amo, *Prog. Org. Coat.* **1999**, *36*, 211.
[4] C. H. Hare, *J. Prot. Coat. Minings* **1998**, *15*, 31.
[5] G. A. Howard, *Pigment Resins Technol.* **2000**, *29*, 325.
[6] G. Meyer, *Farbe Lack* **1963**, *69*, 528.
[7] M. F. Clay, G. H. Cox, *J. Oil Colour Chem. Assoc.* **1973**, *56*, 13.
[8] G. Meyer, *Farbe Lack* **1965**, *71*, 113.
[9] G. Adrian, A. Bittner, *J. Coat. Technol.* **1986**, *58*, 59.
[10] R. Romagnoli, V. F. Vetere, *Corrosion* **1995**, *51*, 216.
[11] J. A. Burkill, J. E. O. Mayne, *Surf. Coat. Int.* **1988**, *71*, 273.
[12] A. Amidurin, C. Barreau, R. Hellouin, D. Thierry, *Prog. Org. Coat.* **1995**, *25*, 339.
[13] B. Del Amo, R. Romagnoli, V. F. Vetere, L. S. Hernández, *Prog. Org. Coat.* **1998**, *33*, 28.

© 2004 Wiley-VCH Verlag GmbH & Co. KGaA, Weinheim

[14] H. M. A. Al-Maydama, P. J. Gardner, I. W. McAra, *Thermochim. Acta* **1992**, *194*, 117.
[15] M. Eisenberger, M. Addy, A. Rossbach, *J. Dent.* **2003**, *31*, 137.
[16] R. Nomoto, K. Uchida, Y. Momoi, J. F. McCabe, *Dent. Mater.* **2003**, *19*, 240.
[17] R. G. Craig in *Restorative Dental Materials*, Mosby, St. Louis, **1993**.
[18] A. D. Wilson, J. W. Nicholson in *Chemistry of Solid State Material, Vol. 3: Acid-Based Cements, their Biomedical and Industrial Applications*, Cambridge University Press, Cambridge, **1993**.
[19] C. L. Davidson, *Adv. Eng. Mater.* **2001**, *3*, 763.
[20] F. Bohlsen, M. Kern, *Quintessence Int.* **2003**, *34*(7), 493.
[21] R. S. Squier, J. R. Agar, J. P. Duncan T. D. Taylor, *Int. J. Oral Maxillofac Implants* **2001**, *16*, 793.
[22] N. Attar, L. E. Tam, D. McComb, *J. Prosthet. Dent.* **2003**, *89*, 127.
[23] K. A. Proos, M. V. Swain, J. Ironside G. P. Steven *Int. J. Prosthodont.* **2003**, *16*, 82.
[24] B. Czarnecka, H. Limanowska-Shaw, J. W. Nicholson, *J. Mater. Sci.: Mater. Med.* **2003**, *14*, 601.
[25] K. Sunnegardh-Gronberg, A. Peutzfeldt, J. W. V. van Dijken, *J. Dent. Res.* **2002**, *81* (Special Issue B), B361.
[26] E. Mezzomo, F. Massa, S. Libera, *Quintessence Int.* **2003**, *34*, 301.
[27] M. Eisenberger, M. Addy, A. Rossbach, *J. Dent.* **2003**, *31*, 137
[28] T. E. Gier, G. D. Stucky, *Nature* **1991**, *349*, 508.
[29] W. Liu, Y. Liu, Z. Shi, W. Pang, *J. Mater. Chem.* **2000**, *10*, 451.
[30] A. K. Cheetham, G. Ferey, T. Loiseau, *Angew. Chem.* **1999**, *111*, 3466 – 3492; *Angew. Chem. Int. Ed.* **1999**, *38*, 3268 – 3292.
[31] S. Oliver, A. Kuperman, G. A. Ozin, *Angew. Chem.* **1998**, *110*, 48; *Angew. Chem. Int. Ed.* **1998**, *37*, 46.
[32] J. Li, J. Yu, W. Yan, Y. Xu, W. Xu, S. Qiu, R. Xu, *Chem. Mater.* **1999**, *11*, 2600.
[33] L. S. Hernández, G. Garcia, C. López, B. Del Amo, R. Romagnoli, *Surf. Coat. Int.* **1998**, *81*, 19.
[34] P. J. Gardner, I. W. McArn, V. Bartob, G. M. Seydt, *Surf. Coat. Int.* **1990**, *74*, 16.
[35] O. Pawlig, R. Trettin, *Mater. Res. Bull.* **1999**, *34*, 1959.
[36] N. Ewoldsen, R. S. Demke, *Am. J. Orthod. Dentofac.* **2001**, *120*, 45.
[37] C. A. Mitchell, M. Abbariki, J. F. Orr, *Dent. Mater.* **2000**, *16*, 198.
[38] M. V. Goloshchapov, T. N. Filatova, *Russ. J. Inorg. Chem.* **1969**, *14*, 424.
[39] E. A. Nikonenko, I. N. Marenkova, *Russ. J. Inorg. Chem.* **1986**, *31*, 397.
[40] A. Whitaker, *J. Appl. Crystallogr.* **1973**, *6*, 495.
[41] A. Echavaria, A. Simon-Masseron, J. L. Paillaud, V. Gramlich, C. Saldarriaga, *Inorg. Chim. Acta* **2003**, *343*, 51.
[42] J. E. Harwood, R. A. Van Steederen, A. L. Kühn, *Water Res.* **1969**, *3*, 417.
[43] O. V. Yakubovich, O. V. Karmova, O. V. Dimitrova, W. Massa, *Acta. Crystallogr. Sect. C* **1999**, *55*, 151.
[44] J. E. Salmon, H. T. Terrey, *J. Chem. Soc.* **1950**, 2813.
[45] Cards 37-465 and 39-1352, JCPDS–ICDD database, FIZ Karlsruhe, **1996**
[46] O. Pawlig, V. Schellenberger, H. D. Lutz, R. Trettin, *Spectrochim. Acta Part A* **2001**, *57*, 581.
[47] K. Nakamoto in *IR and Raman Spectra of Inorganic and Coordination Compounds*, Wiley, New York, **1986**.
[48] R. J. Hill, J. B. Jones, *Am. Mineral.* **1976**, *61*, 987.
[49] H. D. Lutz, J. Himmrich, M. Schmidt, *J. Alloys Compd.* **1996**, *241*, 1.
[50] V. Petrusevski, B. Soptrajanov, *J. Mol. Struct.* **1988**, *17*, 349.
[51] H. D. Lutz, *Struct. Bonding* **1988**, *69*, 7.
[52] O. Pawlig, R. Trettin, *Chem. Mater.* **2000**, *12*, 1279.
[53] Y. Arnaud, E. Sahakian, M. Romand, J. C. Charbonnier, *Appl. Surf. Sci.* **1988**, *32*, 281.
[54] Y. Arnaud, E. Sahakian, J. Lenoir, A. Roche, *Appl. Surf. Sci.* **1988**, *32*, 296.
[55] J. Komrska, V. Satava, *Silikaty* **1969**, *13*, 135.
[56] H. Haidara, Ph.D. Thesis, University of Muhlhouse (France), **1985**.
[57] E. A. Nikonenko, I. I. Olikov, I. N. Marenkova, L. N. Margolin, L. A. Reznikova, *Russ. J. Inorg. Chem.* **1985**, *30*, 25.
[58] Y. Cudennec, A. Lecerf, A. Riou, Y. Gerault, *C. R. Acad. Sci. Ser. II* **1985**, *30*, 93.
[59] A. Bensalem, *J. Solid State Chem.* **2001**, *162*, 29.
[60] A. B. Yaroslavtsev, Z. N. Prozoroskaya, V. F. Chuvaev, *Zh. Neorg. Khim.* **1989**, *34*, 2036.
[61] E. A. Nikonenko, I. N. Marenkova, *Russ. J. Inorg. Chem.* **1986**, *31*, 397.
[62] M. A. Al-Maydama, P. J. Gardner, I. W. McAra, *Thermochim. Acta* **1992**, *196*, 117.
[63] A. Whitaker, *Acta Crystallogr. Sect. B* **1975**, *31*, 2026.
[64] R. J. Hill, J. B. Jones, *Am. Mineralogist* **1975**, *61*, 987.
[65] A. Okuwary, J. Ninagawa, T. Okabe, K. Omori, *Bull. Chem. Soc. Jpn.* **1972**, *45*, 1720.
[66] R. S. Gamidov, V. P. Galovachev, *Dokl. Akad. Nauk SSSR* **1963**, *150*, 381.
[67] T. J. White, D. ZhiLi, *Acta Crystallogr. Sect. B* **2003**, *59*, 1.
[68] J. S. Stephens, C. Calvo, *Can. J. Chem.* **1967**, *45* 2303.
[69] J. S. Stephens, C. Calvo, *Can. J. Chem.* **1965**, *43*, 436.
[70] L. J. Spencer, *Miner. Mag.* **1908**, *38*, 1.
[71] G. C. Pimentel, A. L. McClellan, *The Hydrogen Bond*, Freeman, New York, **1960**.
[72] I. Kumbasar, J. J. Finney, *J. Mineral. Soc.* **1968**, *36*, 88.
[73] G. Y. Chao, *Z. Kristallogr.* **1969**, *130*, 261.

Received: November 6, 2003

Published online: April 22, 2004

 © 2004 Wiley-VCH Verlag GmbH & Co. KGaA, Weinheim